the simulation servo system. Six panel-mounted voltmeters are used to read out analog axes position and rate information.

Sensor Stimulation

A high-current, carbon arc lamp with a properly designed lens system is used as the sun simulator to provide a reasonable near-optimum source. For certain spacecraft control modes, sunlight impinging from a nearly vertical direction is required. For this condition a large, front-surface mirror, oriented as shown in Fig. 1, is used to reflect the light from an arc lamp mounted on an elevated platform onto the test vehicle. For other control modes, the sun simulator in the lower position of Fig. 1 may be required. In this location the arc lamp can be more closely coupled to the test package, and a higher intensity light is obtained. The facility is sufficiently versatile to permit other orientations of the solar simulator if appropriate. Solar constants from 0.2 to 1.0 have been obtained with an apparent source size or collimation at the sensor of approximately 0.5°. This type of solar simulation has proven to be quite satisfactory for the control systems evaluated to date.

For many spacecraft missions, Polaris forms an ideal reference for precise pointing maneuvers. The star simulator used in this facility provides a replica of the +2.1 visual magnitude of this star with an F8 spectral characteristic. It consists of a small light source positioned at the focal point of a 15-in.-diam parabolic mirror with a focal length of 40 in. The intensity of the light source can be varied from +6 to −2 magnitude by the selection of the proper neutral density filter for the excitation lamp.

The earth simulator (Fig. 7) for this particular control evaluation has been configured to that seen by a spacecraft which is orbiting at synchronous altitude (approximately 20,000 naut miles) where the angle subtended by earth is about 18°. By proper design, other sizes of earth can be simulated if required. The earth sensor used in one control system evaluated, sensed radiation in the 20- to 40-μ infrared band and the simulated target was designed to duplicate the

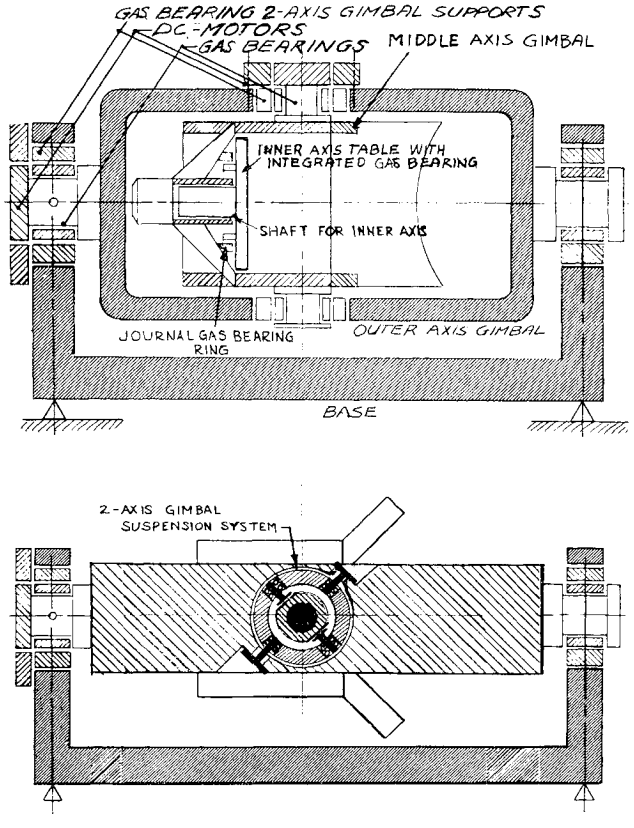

Fig. 6 Gas bearing suspension system.

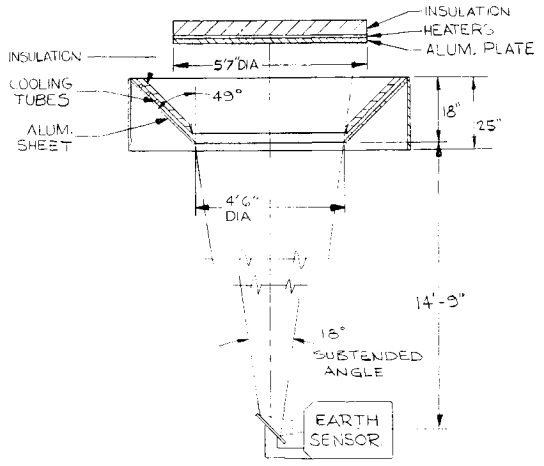

Fig. 7 Earth simulator configuration.

earth's irradiance energy in this band against a deep space background. The background in the simulated earth system is nominally at room temperature. The inner diameter of the background determines the subtended limb of the simulated earth as observed by the sensor. The temperature of the earth target (an aluminum disk with surface heaters bonded to the back side) can be varied up to 360°F. The front side is coated to provide high emissivity. The simulated space background consists of a coated (to provide high emissivity), truncated conical section of aluminum sheet to which a spiral of tubing is bonded. Cooling or heating liquid may be circulated through this tubing. The cone half-angle and length of cylindrical section were selected to prevent single specular reflections of energy radiation from any source in the facility within the space background field-of-view of the sensor.

Summary

Thus, a motion simulator facility is provided which permits simulation of in-orbit flight for attitude control performance demonstration by duplicating spacecraft motion and by simulating reference targets.

Influence of Spatial Correlation upon Load Resolution

L. V. Schmidt*
Naval Postgraduate School, Monterey, Calif.

Nomenclature

D	=	reference length on bluff body
$l(x,t)$	=	load per unit length at station x and time t
$L(t)$	=	total load over domain at time t
t	=	time
β	=	$(r - s)/D$ = dimensionless spacing variable
γ	=	r/D = dimensionless distance
τ	=	time lag
ω	=	circular frequency
χ	=	correlation length scale, fraction of D
$\Phi(r,s,\omega)$	=	cospectral density relating station s to station r at frequency ω
$\Psi(r,s,\omega)$	=	quad-spectral density relating station s to station r at frequency ω
$\psi_2(r)$	=	spatial variable in $\Phi(r,s,\omega)$ for two-dimensional flow case

Received October 8, 1969.

* Associate Professor of Aeronautics, Naval Postgraduate School. Associate Fellow AIAA.

$\psi_3(r,s)$ = spatial variable in $\Phi(r,s,\omega)$ for three-dimensional flow case

$\varphi_{2,3}(\omega)$ = frequency variable in $\Phi(r,s,\omega)$ for two- and three-dimensional flow cases, respectively

Introduction

THE character of the flow perpendicular to the symmetry axis of a long slender circular cylinder has been of interest to investigators for over a hundred years. Although the body may appear geometrically to be two-dimensional, the flow can be considered in this manner only from the standpoint of mean or average properties. Time histories of flow properties exhibit three-dimensional features such as typically described by Roshko[1] using hot wires in the wake, el Baroudi[2] using hot wires near to the separation point, Prendergast[3] with static pressure transducers on the cylinder, and Schmidt[4] with sectional load transducers. In all of these measurements, the spatial variation of the particular flow property was characterized by the cross-correlation coefficient at zero time lag that related the output of a fixed to that of a relocatable transducer.

Recent experiments on circular cylinders with harmonic motion in the lateral direction have disclosed that the flow near to the cylinder will become spatially organized when the reduced or nondimensional frequency of the motion approaches or is near to the characteristic Strouhal number of the flow. Strouhal[5] in 1878 described this feature as a tonal reinforcement when the resonant frequency of a taut wire coincided with the characteristic acoustic tone created by the wire in the moving stream. Typically today, pressure measurements by Ferguson and Parkinson[6] and hot-wire measurements by Toebes[7] in the wake near to the oscillating cylinder have amplified upon the early observation of Strouhal by establishing that the vortex shedding mechanism becomes "locked in" by motion with an attendant increase in correlation length of the unsteady flow features.

Jones, Cincotta, and Walker[8] reported on the unsteady lateral force showing an apparent increase in rms value when the circular cylinder used in their experiment was harmonically oscillated at relatively small amplitudes near to the characteristic Strouhal number applicable to the Reynolds number of their investigation. Mortenson and Schmidt[9] also reported on an apparent increase in "average" lift force over a noncircular bluff body with the amount of motion required to bring about the feature being on the order of a few percent of cylinder width.

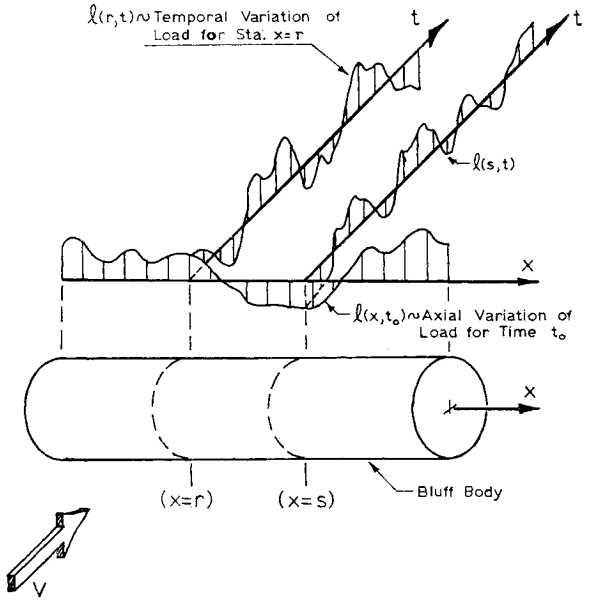

Fig. 1 Spatially varying flowfield.

It is the objective of the analysis described herein to estimate the significance of an improvement in spatial correlation of unsteady sectional loads upon the apparent or "average" load over a finite region as might be indicated by the output of a load cell.

Discussion

In considering the effect of spatial correlation in the axial direction upon the total load measured as a time history over a finite sized region, we shall assume that the local properties as described by the section loading will remain constant from a statistical sense. Figure 1 serves to illustrate the geometry of a two-dimensional body immersed in a moving fluid with the feature of having time varying loads that are three-dimensional in character. Although the loads considered are visualized as being in the lateral (or lift) direction, the arguments presented here are equally applicable to other physical quantities such as drag loads.

At any instant in region (a,b), the total load may be described in terms of the section or distributed load as

$$L(t) = \int_a^b l(x,t)dx \tag{1}$$

The mean square time average of total loading is

$$\langle L^2 \rangle = \lim_{T\to\infty} \frac{1}{2T} \int_{-T}^{+T} \int_a^b \int_a^b l(r,t)l(s,t)dr\,ds\,dt$$

By interchanging the order of integration, the mean square of total loading may be expressed in terms of the cross correlation at zero time lag ($\tau = 0$).

$$\langle L^2 \rangle = \int_a^b \int_a^b \langle ll \rangle_{\substack{r,s \\ \tau=0}} dr\,ds \tag{2}$$

The cross-correlation function for a stationary process can be stated in terms of the co- and quad-spectral density functions as:

$$\langle ll \rangle_{\substack{r,s \\ \tau}} = \int_{-\infty}^{\infty} [\Phi(r,s,\omega) + i\Psi(r,s,\omega)] \exp(i\omega\tau)d\omega \tag{3}$$

where the co- and quad-spectral density functions are recognized as being symmetric and antisymmetric natured respectively with respect to frequency. For time lag, τ, equal to zero, Eq. (3) simplifies by virtue of the symmetry properties to the following:

$$\langle ll \rangle_{\substack{r,s \\ \tau=0}} = 2\int_0^{\infty} \Phi(r,s,\omega)d\omega \tag{4}$$

Since the zero time lag cross-correlation function, as defined in Eq. (4) has a dominant role in establishing the mean square of total loading, Eq. (2), it is possible to make estimates of its influence by assigning or assuming properties of the cospectral density relative to the character of the spatial loading. As will be shown, a separation of variable technique aids in the analysis, however justification of the method is

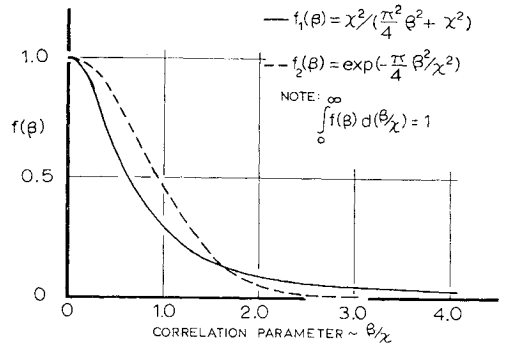

Fig. 2 Spatial variation of ψ_3 function.

based upon convenience and physical intuition rather than rigor.

As a starting point, a perfect spatial correlation that corresponds to a two-dimensional flow assumption would imply that the sectional and total loadings were related in a simple geometrical manner. On the further assumption of isolating the frequency terms from the spatial terms, which is somewhat similar to the analysis of Thomson and Barton,[10] one could approximate the cospectral density function as:

$$\Phi(r,s,\omega) = \tfrac{1}{2}\psi_2(r)\psi_2(s)\varphi_2(\omega) \tag{5a}$$

and consequently

$$\underset{\tau=0}{\langle ll\rangle_{r,s}} = \psi_2(r)\psi_2(s)\int_0^\infty \varphi_2(\omega)d\omega \tag{5b}$$

When Eq. (5b) is substituted into the expression for mean square of total loading, Eq. (2), one obtains that

$$\langle L^2\rangle_2 = \left[\int_a^b \psi_2(r)\,dr\right]^2 \int_0^\infty \varphi_2(\omega)d\omega \tag{5c}$$

Similarly, the three-dimensional case would be approximated as

$$\Phi(r,s,\omega) = \tfrac{1}{2}\psi_3(r,s)\varphi_3(\omega) \tag{6a}$$

$$\underset{\tau=0}{\langle ll\rangle_{r,s}} = \psi_3(r,s)\int_0^\infty \varphi_3(\omega)d\omega \tag{6b}$$

$$\langle L^2\rangle_3 = \int_a^b\int_a^b \psi_3(r,s)dr\,ds\int_0^\infty \varphi_3(\omega)d\omega \tag{6c}$$

Since at station $x = r$, the three-dimensional case must be equivalent to the two-dimensional case from the standpoint of section loadings, it follows that

$$\psi_2^2(r)\int_0^\infty \varphi_2(\omega)d\omega = \psi_3(r,r)\int_0^\infty \varphi_3(\omega)d\omega \tag{7}$$

The assumption of separating the spatial and frequency variables in the cospectral density function implies that the spectral variation would be invariant with spacing or location. As is frequently done, the integral relation of the spectral variation can be normalized to have unit value, hence,

$$\int_0^\infty \varphi_2(\omega)d\omega = \int_0^\infty \varphi_3(\omega)d\omega = 1 \tag{8a}$$

and therefore,

$$\underset{\tau=0}{\langle ll\rangle_{r,r}} = \psi_2^2(r) = \psi_3(r,r) \tag{8b}$$

The spacing variable $\psi_3(r,s)$ can be reexpressed in terms of reference location, r, and relative spacing, $(r - s)$. It is convenient to normalize these variables with respect to reference length (typically a diameter or frontal height) and redefine the spacing variable in terms of γ and β, respectively. In addition, one may establish a scale of spatial correlation, χ, which is defined by the relation that

$$\int_0^\infty \psi_3(\gamma,\beta)d\beta = \chi\underset{\tau=0}{\langle ll\rangle_{r,r}} \tag{9}$$

Requirements placed upon the spacing variable in addition to those that assure the existence of Eq. (9) are that:

1) at $\gamma = r/D$, $\beta = 0$; $\psi_3(\gamma,0) = \underset{\tau=0}{\langle ll\rangle_{r,r}}$

2) at $\gamma = r/D$, $\beta = \infty$; $\psi_3(\gamma,\infty) = 0$

3) symmetry; $\psi_3(\gamma,+\beta) = \psi_3(\gamma,-\beta)$

Two forms of the ψ_3 function will be considered that satisfy the above requirements, the first being a quadratic expression, while the second will be a normal distribution type of exponential function. Let

$$\psi_3(\gamma,\beta) = f(\beta)\underset{\tau=0}{\langle ll\rangle_{r,r}}$$

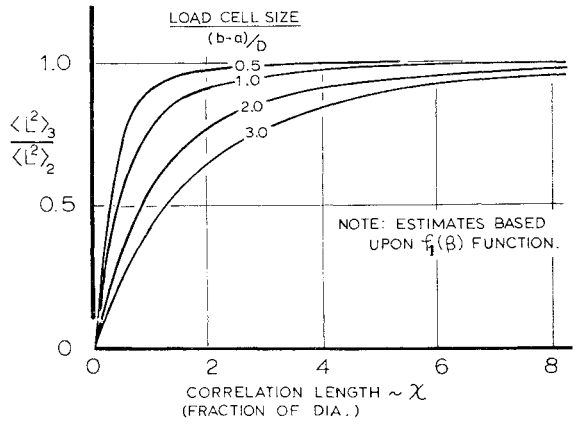

Fig. 3 Transducer effectiveness (quadratic ψ_3 function).

and assign

$$f_1(\beta) = \chi^2/[(\pi^2/4)\beta^2 + \chi^2] \tag{10a}$$

$$f_2(\beta) = \exp[-(\pi/4)\beta^2/\chi^2] \tag{10b}$$

These expressions, which are compared on Fig. 2, may be used to evaluate the net lift over a domain and allow comparison between three- and two-dimensional situations. Combining Eqs. (5c) and (6c) yields that:

$$\frac{\langle L^2\rangle_3}{\langle L^2\rangle_2} = \frac{\int_a^b\int_a^b \psi_3(r,s)dr\,ds\int_0^\infty \varphi_3(\omega)d\omega}{\left[\int_a^b \psi_2(r)dr\right]^2\int_0^\infty \varphi_2(\omega)d\omega} \tag{11}$$

which simplifies to the form that:

$$\frac{\langle L^2\rangle_3}{\langle L^2\rangle_2} = \int_{a/D}^{b/D}\int_{(\gamma-b/D)}^{(\gamma-a/D)} f(\beta)d\gamma d\beta \tag{12}$$

After substitution of the functionals $f_1(\beta)$ and $f_2(\beta)$ into Eq. (12), solutions for the two cases may be obtained after a little bit of algebraic reduction to yield that

case 1: using $f_1(\beta)$

$$\langle L^2\rangle_3/\langle L^2\rangle_2 = 2(\tan^{-1}\alpha/\alpha) - (1/\alpha^2)\ln(1+\alpha^2) \tag{13}$$

where

$$\alpha = (\pi/2)(b-a)/\chi D$$

case 2: using $f_2(\beta)$

$$\langle L^2\rangle_3/\langle L^2\rangle_2 = (\pi/\alpha)\,\mathrm{erf}(\alpha/(\pi)^{1/2}) - (\pi/\alpha^2)[1-\exp(-\alpha^2/\pi)] \tag{14}$$

where the error function is defined as

$$\mathrm{erf}(x) = \frac{2}{(\pi)^{1/2}}\int_0^x \exp(-u^2)du$$

It may easily be shown that in the limit as the term α tends to zero, Eqs. (13) and (14) both tend to a value of unity. Physically speaking, this corresponds to having a striplike load cell whose width is much less than the correlation length scale with the result that the load cell would be able to sense or resolve the true sectional loading.

Equations (13) and (14) are shown on Figs. 3 and 4, respectively, as a function of correlation length scale for various sized sensing domains, and the meaning of the results are comparable. For example, if the spatial function were defined by $f_1(\beta)$, the load cell extended for a 2.0-diam axial distance, and the spatial correlation length were one diameter (a value in accord with the results of Schmidt[4]), then the load cell would have a mean square output of approximately 56% of the true sectional loading value. Furthermore, if the flowfield became spatially correlated due to an external unifying influence such as motion so that the correlation length increased to (say) four cylinder diameters, then the load cell

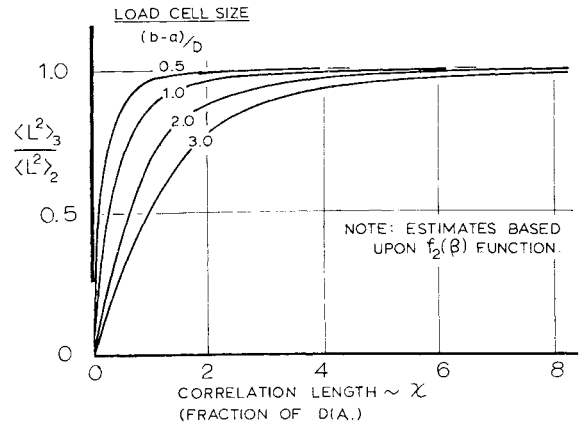

Fig. 4 Transducer effectiveness (exponential ψ_3 function).

output would be increased by approximately 63% relative to the original reading.

Concluding Remarks

The spatial resolution achieved with a sensing element depends upon its actual size relative to a cross-correlation length scale. The sample situations considered herein provide one with a quantitative measure of this relationship. In addition, recent improvements in data retrieval and analysis methods make feasible the consideration of greater statistical detail, which in turn requires that more attention be paid to the spatial resolution of the sensing elements.

Recent research on unsteady loads about bluff bodies has led to a much clearer understanding of three-dimensional flow traits and the manner in which motion can act to unify flow features which otherwise would be disorderly. However, the details of how motion acts to increase section loadings and improve spatial correlations still remains to be defined, and in particular, it is not clear whether this will only occur very near a particular nondimensional frequency that depends upon geometrical shape. When these matters are understood, it will be necessary to have workable methods for predicting structural response to random, motion-dependent inputs.

References

[1] Roshko, A., "On the Development of Turbulent Wakes from Vortex Streets," TR 1191, 1954, NACA.

[2] el Baroudi, M. Y., "Measurements of Two-Point Correlations of Velocity Near a Circular Cylinder Shedding a Karman Vortex Street," UTIA TN 31, 1960, Univ. of Toronto.

[3] Prendergast, V., "Measurement of Two-Point Correlations of the Surface Pressure on a Circular Cylinder," UTIA TN 23, 1958, Univ. of Toronto.

[4] Schmidt, L. V., "Measurement of Fluctuating Air Loads on a Circular Cylinder," *Journal of Aircraft*, Vol. 2, No. 1, Jan.-Feb. 1965, pp. 49–55.

[5] Strouhal, V., "Uber eine Besondre Art der Tonerregung," Wied. Ann. Physik u. Chem., Neue Folge, Band V, 1878, pp. 216–251.

[6] Ferguson, N. and Parkinson, G. V., "Surface and Wake Flow Phenomena of the Vortex-Excited Oscillation of a Circular Cylinder," paper 67-VIBR-31, 1967, American Society of Mechanical Engineers.

[7] Toebes, G. H., "The Unsteady Flow and Wake Near an Oscillating Cylinder," paper 68-WA/FE-23, 1968, American Society of Mechanical Engineers.

[8] Jones, G. W., Cincotta, J. J., and Walker, R. W., "Aerodynamic Forces on a Stationary and Oscillating Circular Cylinder at High Reynolds Numbers," TR R-300, 1969, NASA.

[9] Mortenson, W. P. and Schmidt, L. V., "Aeroelastic Problems as Found in a Large Antenna System," paper 67-VIBR-39, 1967, American Society of Mechanical Engineers.

[10] Thomson, W. T. and Barton, M. V., "The Response of Mechanical Systems to Random Excitations," *Journal of Applied Mechanics*, Vol. 24, 1957, pp. 248–251.

Nonlinear Analysis of a Launch Vehicle Attitude Control System

SHERMAN M. SELTZER*
George C. Marshall Space Flight Center, Huntsville, Ala.

AN attitude control system for a large space vehicle was postulated for use during ascent through the denser portion of the Earth's atmosphere. Subsequently this system was modified by the addition of a nonlinear element and analyzed to determine its suitability for continued use after the vehicle had risen above the denser portion of the atmosphere and the guidance loop had closed.[1] Using a Nyquist plot and a describing function linearization, it was determined that a range of control system gains could be chosen that precluded limit cycle operation and ensured stable operation. The low pass nature of the transfer function under investigation lends itself well to utilization of describing function techniques. Subsequent analysis has indicated that, due to some incorrect considerations, there was a range of initial conditions that could excite unstable sustained oscillation. In this Note, this range of initial conditions will be portrayed in a parameter space, and it will be shown how this range can be computed numerically. In addition, a new result will be shown in the sense that a stable region of two control system gains will be established using a single unified method for both the nonlinear and the linear portions of the analysis without recourse to the Nyquist plot previously used. The parameter method provides adjustment of two (rather than one, as with the Nyquist technique) gains in the investigation of sustained oscillations and stable operation which is a significant advantage in this problem.

As shown, the transfer function of the linear portion of the system is

$$G(s) = \frac{(a_0s^2 + k_1s + k_2)(s^2 - c)}{s^3(s^3/\omega^2 + 2\zeta_e s^2/\omega_e + s + a_1c)} \quad (1)$$

The characteristic equation of the linearized system (Fig. 1, Ref. 1) is

$$B(s) + G_D(A)C(s) = 0 \quad (2)$$

where $G_D(A)$ is the describing function of the nonlinear element with a saturation characteristic. Specifying the variable parameters as $\epsilon \equiv k_2G_D(A)$ and $\eta \equiv G_D(A)$, one obtains from Eq. (2) the $\zeta = 0$ curve on the parameter plane diagrams of Fig. 1. As known,[2] the existence of limit cycles is indicated at intersections of the $\zeta = 0$ curve which determines the stable region and the M-locus which represents the variation of the describing function $G_D(A)$ in the parameter plane. The other bound of the stable region is defined by the real root boundary which in this case is the η-axis. Stable operation is predicted for those amplitudes (values of $A < A_{LC}$ where A_{LC} is the amplitude of the limit cycle) for which a portion of the describing function line lies within the stable region. If A becomes large enough ($A > A_{LC}$) to cause operation to occur outside the stable region, instability is indicated. Since the slope of the describing function line is k_2, it is seen that a greater portion of that line (and hence a wider range of initial conditions, i.e., initial amplitudes, A) can be made to lie within the stable region as k_2 is decreased in magnitude. Hence a restriction on admissible initial conditions is apparent that was not brought out in Ref. 1.

Received October 15, 1969. Presented as paper II—D1 at the Joint Automatic Control Conference, University of Colorado, Boulder, Colo., August 5–7, 1969.

* Senior Research Engineer, Astrionics Laboratory. Associate Fellow AIAA.